Vibrational Echoes: Dephasing, Rephasing, and the Stability of Classical Trajectories[†]

W. G. Noid, Gregory S. Ezra,* and Roger F. Loring*

Department of Chemistry and Chemical Biology, Baker Laboratory, Cornell University, Ithaca, New York 14853

Received: September 15, 2003

The experimental observables in coherent, multiple pulse infrared spectroscopic measurements can be calculated from the nonlinear response functions describing the nuclear dynamics of molecular and condensed phase systems. Within classical mechanics, these nonlinear response functions can be expressed in terms of the monodromy matrices that quantify the stability of classical trajectories. We use an ensemble of noninteracting, anharmonic oscillators to examine the effects of the divergence in time of the classical stability matrix on the analytic properties of the third-order response function, relevant to vibrational echo spectroscopy. The two-pulse echo measurement is designed to *rephase* a macroscopic variable, that is, to reverse the effects of destructive interference among the dynamics of microscopic systems characterized by a static distribution of energies. Within classical mechanics, this rephasing is shown to preserve the growth with time of the nonlinear response function that is the signature of the divergence of nearby trajectories. For systems with nearly classical nuclear motions, the vibrational echo measurement may then be interpreted as a probe of the stability of atomic trajectories.

I. Introduction

Observables in nonlinear infrared and Raman measurements[1−7] of nuclear motions may be computed from nonlinear response functions characterizing the material system. The challenges posed by computing nonlinear response functions for large anharmonic systems with time-dependent quantum mechanics has motivated the analysis of these quantities within classical mechanics.[8−17] Nonlinear response functions of a classical mechanical system may not be calculated directly from a conventional, equilibrium molecular dynamics simulation, because their computation requires knowledge of stability matrices,[8] which quantify the effects of small deviations in initial conditions on classical trajectories. An alternative to simulating nonlinear response functions, which obviates the need to compute stability matrices, is to perform a nonequilibrium molecular dynamics simulation of the material system in the presence of an electromagnetic field and to evaluate numerically the appropriate low-field limit.[15−17] The relevance of stability matrices to nonlinear optical measurements is intuitively clear. Consider, for example, an anharmonic oscillator coupled to an electric field with an electric dipole interaction. The nonlinear response function quantifies the impulse response of the system. Within classical mechanics, the effect of a short electric field pulse on a dipolar oscillator is the perturbation of the momentum of the oscillator. The nonlinear response function in classical mechanics describes the alteration of classical trajectories by a sequence of such momentum changes.

Classical stability matrices diverge in time, exponentially for a chaotic system and linearly for an integrable one, representing the large effect on a trajectory at long times of a small change in initial conditions.[18] Because classical mechanical nonlinear response functions are expressible as averages over these quantities, the effect of these divergences on the analytical properties of the response functions must be ascertained.

Divergence in time of the response functions would suggest a lack of validity of the perturbation theory in the radiation−matter interaction that produced them.[19] Leegwater and Muka-mel[20] have carried out such analysis in a numerical study of the two-pulse vibrational echo from an ensemble of noninter-acting quartic oscillators. The stability matrices of this integrable system diverge linearly with time.[21] For a microcanonical ensemble, the third-order response function $R^{(3)}(t_3, t_2, t_1)$ diverges linearly in t_1 for increasing t_1 at fixed t_3 and $t_2 = 0$. However, this divergence is removed by thermal averaging for a canonical ensemble of oscillators. The response at each energy within the canonical distribution is linearly divergent in time, but the average of this dependence over a Boltzmann distribution yields a result that does not increase at long times. This phenomenon can be viewed as an example of dephasing: destructive interference between dynamics of different members of an ensemble.

The two-pulse echo experiment in magnetic resonance, optical, or vibrational spectroscopy is designed to reverse the effects of dephasing in a macroscopic magnetization or electric polarization caused by static distributions of energy.[22,23] This *rephasing* can be manifest in $R^{(3)}(t_3, 0, t_1)$ close to the echo condition, $t_3 = t_1$. The model studied by Leegwater and Mukamel, a thermal distribution of uncoupled anharmonic oscillators, may be viewed as displaying static spectral line broadening.[24] The focus of our work is the question of whether the dephasing observed by Leegwater and Mukamel can be rephased by the echo pulse sequence, resulting in a nonlinear response function $R^{(3)}(t, 0, t)$ that diverges with increasing t, even for a canonical ensemble of oscillators. We present below both numerical and analytical arguments that support the existence of such a temporal divergence. Our findings suggest that, within the domain of classical mechanics, infrared pulse sequences can provide a sensitive probe of the stabilities of classical trajectories, even for a system in thermodynamic equilibrium. This classical interpretation of the vibrational echo

Vibrational Echoes

J. Phys. Chem. B, Vol. 108, No. 21, 2004 **6537**

can be usefully applied to quantum systems that are near the classical limit. The third-order response function, the vibrational echo observable, and our model are described in section II, numerical results are discussed in section III, analytical treatments are presented in section IV, and implications of this work are summarized in section V. A diagrammatic representation of the classical response function, which identifies the classical analogues of quantum mechanical dephasing and rephasing processes, is presented in the Appendix.

II. Quantum and Classical Vibrational Echoes

The observable in a vibrational echo measurement may be computed from the third-order optical response function $R^{(3)}(t_3, t_2, t_1)$, which is defined by[25]

$$P^{(3)}(t) = \int_0^\infty dt_3 \int_0^\infty dt_2 \int_0^\infty dt_1\, R^{(3)}(t_3, t_2, t_1) E(t - t_3) \times$$
$$E(t - t_2 - t_3) E(t - t_1 - t_2 - t_3) \quad (2.1)$$

in which $E(t)$ denotes the electric field amplitude, $P^{(3)}(t)$ is the macroscopic electric polarization, and $\{t_j\}$ are the elapsed times between successive radiation−matter interactions. With the neglect of propagation effects, the signal in an echo experiment may be computed from the square of the appropriately phase-matched component of the polarization.[25] In a two-pulse echo measurement, in the limit of impulsive excitation, the observable is related to the response function with the second time set to zero, $R^{(3)}(t_3, 0, t_1)$.[25] For a radiation−matter interaction of the electric dipole form, $R^{(3)}$ may be expressed as an average of three nested commutators[25]

$$R^{(3)}(t_3, t_2, t_1) = \left(\frac{i}{\hbar}\right)^3 \langle [[[\hat{q}(t_1 + t_2 + t_3), \hat{q}(t_1 + t_2)], \hat{q}(t_1)],$$
$$\hat{q}(0)]\rangle \quad (2.2)$$

The electric dipole operator is taken to be proportional to the coordinate operator $\hat{q}$ governing an "active" degree of freedom that interacts with the electric field, and the coefficient of proportionality is suppressed. Other "dark" degrees of freedom may couple to $\hat{q}$. The coordinate operator in the Heisenberg picture is denoted $\hat{q}(t)$, and the angular brackets represent an average over the appropriate density operator. The classical mechanical expression for $R^{(3)}$ may be obtained from the $\hbar \rightarrow 0$ limit of eq 2.2, or, equivalently, from carrying out time-dependent perturbation theory within classical mechanics[8]

$$R^{(3)}_{cl}(t_3, t_2, t_1) = -\langle \{\{\{q(t_1 + t_2 + t_3), q(t_1 + t_2)\}, q(t_1)\},$$
$$q(0)\}\rangle \quad (2.3)$$

The classical coordinate interacting with the radiation field is denoted $q(t)$, $\{\cdots, \cdots\}$ are Poisson brackets, and $\langle\cdots\rangle$ denotes an average over the classical phase space distribution. If this distribution is taken to have the canonical form, then the classical response function can be written as[12]

$$R^{(3)}_{cl}(t_3, t_2, t_1) = -\frac{\beta}{m}\Big[\langle \mathbf{M}_{qp}(t_3, t_2) \mathbf{M}_{pp}(-t_1, 0)\rangle -$$
$$\frac{\beta}{m}\langle \mathbf{M}_{qp}(t_3, t_2) p(-t_1) p(0)\rangle\Big] \quad (2.4)$$

The momentum conjugate to q is p, the mass associated with coordinate q is m, $\beta \equiv 1/k_B T$, and the elements of the stability matrix are defined by, for example,

$$\mathbf{M}_{qp}(t_a, t_b) \equiv \frac{\partial q(t_a + t_b)}{\partial p(t_b)} \quad (2.5)$$

The partial derivative in eq 2.5 is taken with the coordinates and momenta of the other degrees of freedom held fixed.

We will consider the classical and quantum mechanical response functions for a thermal ensemble of noninteracting Morse oscillators,[24] each with Hamiltonian

$$H = \frac{p^2}{2m} + D(1 - e^{-\alpha q})^2 \quad (2.6)$$

The quantum response function may be calculated directly from eq 2.2 by evaluating the trace in the energy representation.[26,27] Calculation of the classical response function is most conveniently performed using the action-angle variables for the Morse oscillator[21,27] (I, θ). The Hamiltonian, coordinate, and momentum are expressed in terms of these variables as follows

$$H = \omega I - \frac{I^2 \omega^2}{4D}, \quad I \leq 2D/\omega \quad (2.7)$$

$$q(I, \theta) = \sqrt{\frac{2D}{m\omega^2}} \ln\left[\frac{1 + \sqrt{H(I)/D}\cos\theta}{1 - H(I)/D}\right] \quad (2.8)$$

$$p(I, \theta) = -\sqrt{2mD}\frac{\sqrt{H(I)/D - (H(I)/D)^2}\sin\theta}{1 + \sqrt{H(I)/D}\cos\theta} \quad (2.9)$$

These variables are propagated according to

$$I(t) = I(0) \quad (2.10)$$

$$\theta(t) = \theta(0) + \bar{\omega}(I)t \quad (2.11)$$

$$\bar{\omega}(I) = \frac{\partial H}{\partial I} = \omega\left(1 - \frac{I\omega}{2D}\right) \quad (2.12)$$

An action-dependent frequency, $\bar{\omega}(I)$, is defined in eq 2.12.

For the Morse oscillator, the quantum mechanical response function takes the form

$$R^{(3)}(t_3, 0, t_1) = (m^2 \omega D)^{-1} F(\omega t_1, \omega t_3; \beta D, \beta \hbar \omega) \quad (2.13)$$

$$\omega \equiv \alpha\sqrt{\frac{2D}{m}} \quad (2.14)$$

The response function is expressible as the product of a dimensional factor, $(m^2 \omega D)^{-1}$, and a dimensionless function of time variables scaled by the harmonic frequency, ω, and of two temperature-dependent parameters: the classical mechanical βD and the quantum mechanical $\beta \hbar \omega$. The classical response function, $R^{(3)}_{cl}$ is the $\hbar \rightarrow 0$ limit of eq 2.13 and hence can be written as a dimensionless quantity depending on time variables only through ωt_1 and ωt_3 and on temperature only through βD. In numerical calculations shown below, time variables are scaled by ω and $R^{(3)}$ is shown as the quantity $F \equiv m^2 \omega D R^{(3)}$.

III. Dephasing and Rephasing in a Canonical Ensemble

The dependence of the classical mechanical echo response function, $R^{(3)}_{cl}(t_3, 0, t_1)$ on t_3 at fixed t_1 for a thermal distribution of noninteracting Morse oscillators is shown in Figure 1. In a two-pulse vibrational echo measurement in the limit of impulsive excitation, t_1 corresponds to the experimentally controlled delay time between applied laser pulses and t_3 corresponds to the
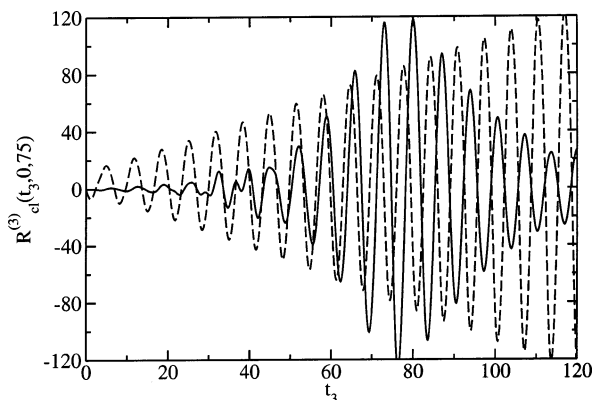
Figure 1. The classical mechanical third-order response function, $R_{cl}^{(3)}(t_3, 0, t_1)$, is shown as a function of t_3 for fixed $t_1 = 75$. The solid curve is calculated for a canonical distribution with $\beta D = 12.8$, and the dashed curve shows the contribution to the thermal result for a single energy, $E = 0.078D$.

detection time, which is typically integrated over in an actual measurement. The calculations in Figure 1 were performed using eq 2.4, together with the analytical solution for the dynamics of the Morse oscillator in terms of action-angle variables[24] in eqs 2.7−2.12. In Figure 1, the temperature is given by $\beta D = 12.8$, and $t_1 = 75$. The dashed curve in Figure 1 shows the contribution to the thermally averaged response function from oscillators with a fixed energy, computed by reinterpreting the angular brackets in eq 2.4 as a microcanonical average with $E = 0.078D$. The contribution to $R_{cl}^{(3)}(t_3, 0, t_1)$ from oscillators with a single energy is seen to diverge linearly with t_3, reflecting the linear divergence with time of stability matrix elements for the Morse oscillator.[13,20] The complete thermally averaged $R^{(3)}(t_3, 0, t_1)$ is shown by the solid curve in Figure 1. The weighted sum of divergent contributions from each energy produces a result that does not diverge in time and displays the temporal profile that gives the echo measurement its name, peaked near $t_3 = t_1$. The removal of a similar divergence in t_1 at fixed t_3 by averaging over a thermal distribution was observed in calculations of $R^{(3)}(t_3, 0, t_1)$ for an ensemble of quartic oscillators by Leegwater and Mukamel.[20]

Because the two-pulse echo measurement acts to rephase the destructive interference between contributions to the polarization from different members of an ensemble, we next examine the dependence of the magnitude of $R_{cl}^{(3)}(t_3, 0, t_1)$ at the nominal peak of the echo signal, $t_1 = t_3$, on the delay time. $R_{cl}^{(3)}(t, 0, t)$ is shown in Figure 2 for two temperatures: $\beta D = 25.6$ (dashed curve) and $\beta D = 63.9$ (solid curve). Each plot shows oscillations at a frequency near 2ω superposed on an apparent linear divergence. Also plotted is the temperature-independent line $R^{(3)}(t, 0, t) = -t/2m^2D$, which is seen to represent this apparent linear divergence at both temperatures. We refer to the long-time dependence of $R^{(3)}(t, 0, t)$ shown in Figure 2 as an "apparent" divergence, because these numerical calculations over a finite time range suggest, but do not prove, that $-t/2m^2D$ is the asymptotic $t \rightarrow \infty$ behavior of the response function for this model.

To investigate further the apparent long-time divergence of $R_{cl}^{(3)}(t, 0, t)$ in Figure 2, we compare the classical calculation for $\beta D = 25.6$ to a quantum mechanical calculation for $\beta D = 25.6$ and $\beta \hbar \omega = 4.0$ in Figure 3. The solid curve shows $R_{cl}^{(3)}(t, 0, t)$, reproduced from Figure 2, and the dashed curve shows $R^{(3)}(t, 0, t)$ computed from evaluating the trace in eq 2.2 in the energy representation and truncating sums over states to include only bound states. The quantum curve lacks the apparent
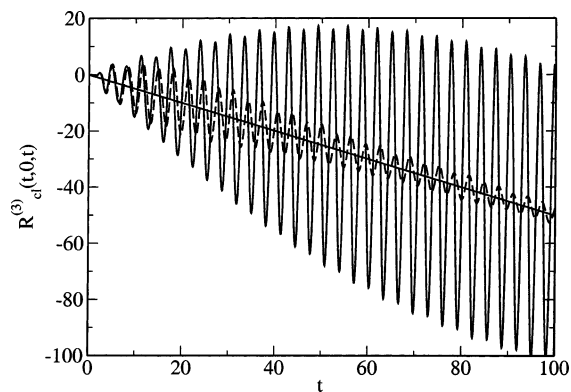

Figure 2. The classical mechanical third-order response function is shown for a thermal ensemble of Morse oscillators at two temperatures: $\beta D = 25.6$ (dashed curve) and $\beta D = 63.9$ (solid curve). The solid line shows the apparent asymptotic divergence, $-t/(2m^2D)$.
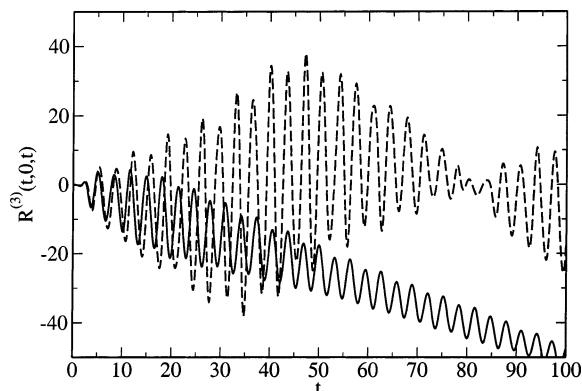

Figure 3. Classical (solid curve) and quantum mechanical (dashed curve) third-order response functions are shown for $\beta D = 25.6$. In the quantum case, $\beta \hbar \omega = 4.0$.

linear divergence of the classical result and is instead characterized by recurrences on a time scale $2\pi/\Delta$, with $\Delta = \hbar \omega^2/2D$ the anharmonic frequency difference between successive one-quantum transitions in the Morse oscillator. For the parameters of Figure 3, $2\pi/\Delta = 80$. For $t \ll 2\pi/\Delta$, the quantum and classical response functions agree. If $\beta \hbar \omega$ is decreased from the value of Figure 3, $2\pi/\Delta$ increases, as does the range of times over which the classical and quantum results agree. The transformation of a slow oscillation whose period increases with decreasing $\hbar$ into a classical divergence in a nonlinear response function for a different model, not characterized by a thermal distribution, has been documented by Wu and Cao.[13]

The calculations shown in Figure 2 suggest that the rephasing property of the vibrational echo preserves at finite temperature a temperature-independent temporal divergence that originates in the stability of individual classical trajectories. We do not present a mathematical proof that, for a thermal ensemble of Morse oscillators, the long-time asymptotic time dependence of the response function is $R_{cl}^{(3)}(t, 0, t) \rightarrow -t/(2m^2D)$. However, our empirical observation of this divergence is supported by approximate, analytic treatments of the quantum and classical mechanical response functions, which provide insight into the physical origin of this time dependence, and which are described in the following section. The particular simplicity of the Morse oscillator raises the question of the generality of this finding, even among one-dimensional anharmonic oscillators. Numerical calculations of $R_{cl}^{(3)}(t, 0, t)$, not shown here, for potentials of the forms $V(q) = bq^4$ and $V(q) = aq^2 + bq^4$, also show a linear divergence, although with a temperature-dependent slope. This result suggests that the linear divergence of $R_{cl}^{(3)}(t, 0, t)$ is not a

Vibrational Echoes

J. Phys. Chem. B, Vol. 108, No. 21, 2004 **6539**

special feature of the Morse oscillator but may be generic to one-dimensional anharmonic oscillators and other integrable systems. The origin of the temperature-independent slope found for the Morse oscillator is discussed in the following section.

IV. Analytical Treatment of the Response Function

In the previous section, we presented numerical calculations of the echo response function of an anharmonic oscillator that showed an apparent linear divergence in time. In support of this finding, we present here an approximate, analytical theory of the classical mechanical third-order response function for a Morse oscillator. We develop this theory in two different ways, first as the $\hbar \to 0$ limit of a quantum mechanical treatment, and second as a result derived wholly within classical mechanics. Each derivation provides a distinct insight into the origin of this temporal divergence.

The quantum mechanical approach is based on the work of Akiyama and Loring,[28] who reported an approximate, analytical theory of the two-pulse vibrational echo for a Morse oscillator coupled to a harmonic solvent. For the present application, we consider this model in the absence of the solvent, in which case the theory results from the three following approximations. The transition moments are evaluated to lowest order in $\hbar$, only single-quantum transitions are considered, and only bound states are included. The third-order response function $R^{(3)}(t_3, 0, t_1)$ is partitioned into a sum of *rephasing* and *nonrephasing* terms. The rephasing terms are characterized by oscillations with the time dependence $\omega(t_1 - t_3)$, which vanish when the echo condition is satisfied, $t_1 = t_3$. These terms also contain temperature-dependent dephasing functions denoted $\{N_j\}$, which are decaying functions of the variable $t_1 - t_3$ and which hence become independent of time under the echo condition. By contrast, the nonrephasing terms contain temporal oscillations with the time dependence $\omega(t_3 + t_1)$ and have temperature-dependent decay factors of the form $N_j(t_1 + t_3)$, which retain their time dependence for any positive values of the time delays t_1 and t_3. These results follow from omitting the solvent relaxation factors in eqs 30 and 34 of ref 28.

$$R^{(3)}(t_3, 0, t_1) = R_{\mathrm{re}}^{(3)}(t_3, 0, t_1) + R_{\mathrm{nr}}^{(3)}(t_3, 0, t_1) \quad (4.1)$$

$$R_{\mathrm{re}}^{(3)}(t_3, 0, t_1) = (2m^2\omega^2\hbar)^{-1} \, \mathrm{Im}[\mathrm{e}^{i\omega(t_3-t_1)}X_{\mathrm{re}}(t_1, t_3) + \\ \mathrm{e}^{-i\omega(t_3-t_1)}Y_{\mathrm{re}}(t_1, t_3)] \quad (4.2)$$

$$X_{\mathrm{re}} = [N_2^*(t_3 - t_1) + N_1^*(t_3 - t_1)][\mathrm{e}^{i\Delta t_1} - 1] + [N_2^*(t_3 - t_1) + \\ 3N_1^*(t_3 - t_1) + 2N_0^*(t_3 - t_1)][\mathrm{e}^{i\Delta(t_1-2t_3)} - 1] \quad (4.3)$$

$$Y_{\mathrm{re}} = 2[N_2(t_3 - t_1) + 2N_1(t_3 - t_1) + \\ N_0(t_3 - t_1)][\mathrm{e}^{i\Delta(t_3-t_1)} - 1] - 4N_2(t_3 - t_1) \sin^2\!\left(\frac{\Delta t_3}{2}\right) + \\ 2iN_1(t_3 - t_1) \sin(\Delta t_3) \quad (4.4)$$

$$R_{\mathrm{nr}}^{(3)}(t_3, 0, t_1) = 2R_{\mathrm{re}}^{(3)}(t_3, 0, -t_1) \quad (4.5)$$

The temperature-dependent dephasing functions N_j are defined by

$$N_j(\tau) = \sum_{n=0}^{n_{\max}} n^j \, \mathrm{e}^{in\Delta\tau} \, \mathrm{e}^{-\beta\epsilon_n} / [\sum_{n=0}^{n_{\max}} \mathrm{e}^{-\beta\epsilon_n}] \quad (4.6)$$

$$\epsilon_n = \hbar\omega(n + {}^1\!/_2) - \hbar(\Delta/2)(n + {}^1\!/_2)^2 \quad (4.7)$$

The anharmonic frequency shift of the Morse oscillator $\Delta = \hbar\omega^2/2D$ has been defined in the previous section. The quantum number associated with the highest energy bound state $n_{\max}$ is given by the largest integer smaller than $\omega/\Delta - {}^1\!/_2$.

For some standard models of nonlinear optics,[25] such as a truncated set of n quantum levels with constant frequencies, the echo observable has no classical limit, because the underlying model has no classical analogue. The vibrational echo for a classical Morse oscillator, however, is perfectly well-defined,[12,28] as shown in the previous section, and the approximate expressions in eqs 4.2 and 4.5 have a finite $\hbar \to 0$ limit. It should be noted that, in this limit, one approximation that produced eqs 4.2 and 4.5 becomes exactly correct: the neglect of higher order terms in $\hbar$ in evaluating transition moments.[28]

Taking the $\hbar \to 0$ limit of $R_{\mathrm{re}}^{(3)}$ in eq 4.2 and of $R_{\mathrm{nr}}^{(3)}$ in eq 4.5 requires the leading order dependence for small $\hbar$ of the temperature-dependent factors $N_j(\tau)$, which may be determined exactly from eq 4.6 by converting the summations to integrals

$$\lim_{\hbar \to 0} N_j(\tau) = (\beta\hbar\omega)^{-j}\bar{N}_j(\tau) \quad (4.8)$$

$$\bar{N}_j(\tau) = \frac{\int_0^{2\beta D} \mathrm{d}y \, y^j \, \mathrm{e}^{-y+y^2/(4\beta D)+iy\omega\tau/(2\beta D)}}{\int_0^{2\beta D} \mathrm{d}y \, \mathrm{e}^{-y+y^2/(4\beta D)}} \quad (4.9)$$

The expressions for $R^{(3)}$ in eqs 4.2 and 4.5 depend on $\hbar$ through the $\hbar$ dependence of N_j in eq 4.6, through the $\hbar$ dependence of factors such as $\mathrm{e}^{i\Delta\tau} - 1$, and through an explicit prefactor of $\hbar^{-1}$. Taking the $\hbar \to 0$ limit in eqs 4.2 and 4.5 requires expanding terms of the form $\mathrm{e}^{i\Delta\tau} - 1$ through order $\hbar^3$ and retaining only the leading $\hbar$ dependence of N_j, shown in eq 4.8. These limits are

$$\lim_{\hbar \to 0} R_{\mathrm{re}}^{(3)}(t_3, 0, t_1) = -\frac{t_3}{2m^2D}\bigg\{\cos\omega\,(t_3 - t_1)\bigg[\bar{N}_0'(t_3 - t_1) - \\ \left(\frac{\omega(2t_3 - t_1)}{2D\beta}\right)\bar{N}_1''(t_3 - t_1) + \left(\frac{\omega^2 t_3(t_1 - t_3)}{8D^2\beta^2}\right)\bar{N}_2'(t_3 - t_1)\bigg] + \\ \sin\omega\,(t_3 - t_1)\bigg[\bar{N}_0''(t_3 - t_1) + \left(\frac{\omega(2t_3 - t_1)}{2D\beta}\right)\bar{N}_1'(t_3 - t_1) + \\ \left(\frac{\omega^2 t_3(t_1 - t_3)}{8D^2\beta^2}\right)\bar{N}_2''(t_3 - t_1)\bigg]\bigg\} \quad (4.10)$$

$$\lim_{\hbar \to 0} R_{\mathrm{nr}}^{(3)}(t_3, 0, t_1) = 2\lim_{\hbar \to 0} R_{\mathrm{re}}^{(3)}(t_3, 0, -t_1) \quad (4.11)$$

Here, $\bar{N}_j = \bar{N}_j' + i\bar{N}_j''$.

For $t_1 = t_3 = t$, the rephasing term in eq 4.10 becomes a simple linear divergence

$$R_{\mathrm{re}}^{(3)}(t, 0, t) = -\frac{t}{2m^2D} \quad (4.12)$$

Calculation of the nonrephasing term in eq 4.11 requires evaluation of the integral in eq 4.9. Because our focus is the nonlinear response of a bound degree of freedom, we restrict our attention to $\beta D \gg 1$, as in Figures 1–3. In this case, the
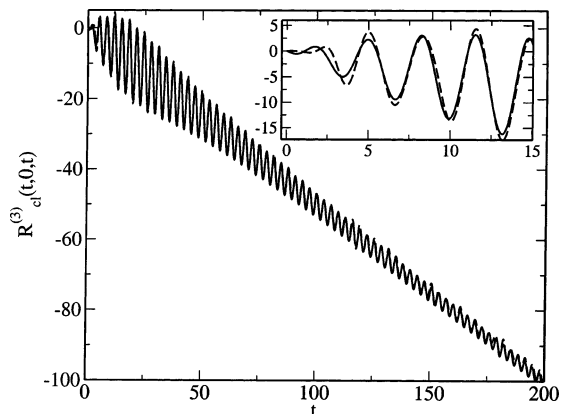
6540 *J. Phys. Chem. B, Vol. 108, No. 21, 2004*

Noid et al.

Figure 4. The classical mechanical third-order response function is shown for $\beta D = 25.6$. The solid curve is the approximation of eqs 4.12 and 4.16, and the dashed curve, nearly indistinguishable on the scale of the larger plot, is computed numerically from eq 2.4. Short-time behavior is shown in the inset.

integral in eq 4.9 can be approximated by replacing the thermal distribution with its harmonic limit.

$$N_0(\tau) \approx \frac{1}{1 - i\dfrac{\omega\tau}{2D\beta}} \quad (4.13)$$

$$N_1(\tau) \approx \frac{1}{\left(1 - i\dfrac{\omega\tau}{2D\beta}\right)^2} \quad (4.14)$$

$$N_2(\tau) \approx \frac{2}{\left(1 - i\dfrac{\omega\tau}{2D\beta}\right)^3} \quad (4.15)$$

Substitution of these results into eq 4.11 yields

$$R_{nr}^{(3)}(t, 0, t) = -\frac{t}{2m^2D}\left\{\cos 2\omega t\left[\frac{2 - 3z^2 - z^4}{(1 + z^2)^3}\right] + \right.$$
$$\left. \sin 2\omega t\left[\frac{z(5 + z^2)}{(1 + z^2)^3}\right]\right\} \quad (4.16)$$

$$z = \frac{\omega t}{D\beta} \quad (4.17)$$

In contrast to the rephasing term in eq 4.12, the nonrephasing contribution to $R^{(3)}(t, 0, t)$ decays to zero, as t^{-1}. To assess the validity of these approximations, we compare in Figure 4 the classical $R^{(3)}(t, 0, t)$ for $\beta D = 25.6$ from Figure 2, the dashed curve, to the prediction of eqs 4.1, 4.12, and 4.16, shown by the solid curve. Except at very short time, as shown in the inset, the approximate result provides a quantitatively accurate representation of the classical response function.

The analytical results in eqs 4.10 and 4.11 provide some insight into the origin of the linear divergence of $R_{cl}^{(3)}(t, 0, t)$ shown in Figures 2−4. As shown in eq 4.12, the rephasing term at $t_1 = t_3 = t$ becomes exactly equal to the apparent asymptotic divergence of $R_{cl}^{(3)}$ in Figure 2, $-t/(2m^2D)$. The nonrephasing term oscillates at 2ω and decays asymptotically to zero as t^{-1}. Thus, although we do not prove that $R_{cl}^{(3)}$ diverges linearly in time, the quantitatively accurate theory of eqs 4.12 and 4.16 displays this feature. The origin of this divergence may be understood within quantum mechanics from consideration of the quantum version of the theory in eqs 4.2 and 4.5. The

quantum vibrational echo from an anharmonic oscillator has been described in the conventional formalism of nonlinear optics in terms of the two-sided Feynman diagrams that depict terms in the radiation−matter perturbation theory.[3,25] Diagrams that contribute to rephasing processes are characterized by a quantum coherence with time dependence $\exp(i\omega't_1)$ followed by a coherence with time dependence $\exp(i\omega''t_3)$, with ω' and ω'' signed frequencies of single-quantum transitions with opposite signs. The product of these factors yields an oscillation with $t_1 - t_3$ at an anharmonic frequency that vanishes as $\hbar \to 0$. For the Morse oscillator, this frequency is $\Delta = \hbar\omega^2/2D$. Individual double-sided Feynman diagrams are not useful in a discussion of the classical $\hbar \to 0$ limit, because their values diverge in this limit, and the classical limit is obtained by combining contributions from different diagrams. The connection between quantum rephasing and the classical time divergence is most easily appreciated by considering the zero-temperature limit of the rephasing term in eq 4.2, which describes a three-level system[3] at $T = 0$.

$$\lim_{T\to 0}R_{re}^{(3)}(t_3, 0, t_1) = \frac{1}{m^2\omega^2\hbar}\{\sin((\omega - \Delta)(t_3 - t_1)) \times$$
$$[\cos\Delta t_3 - 1] - \cos((\omega - \Delta)(t_3 - t_1))[\sin\Delta t_3]\} \quad (4.18)$$

At the echo condition, $t_3 = t_1 = t$, this expression becomes

$$R_{re}^{(3)}(t, 0, t) = -\frac{\sin\Delta t}{m^2\omega^2\hbar} \quad (4.19)$$

Rephasing has removed any time dependence involving the harmonic frequency ω, and the echo signal is predicted[3] to oscillate at the anharmonic frequency Δ. Although this expression describes a quantum system at $T = 0$, it has a finite $\hbar \to 0$ limit, giving precisely the classical mechanical divergence of eq 4.12. A quantum oscillation at an anharmonic frequency is transformed into a linear divergence in classical mechanics.[13]

The classical mechanical results of eqs 4.12 and 4.16 were determined as the $\hbar \to 0$ limit of a quantum mechanical expression. Further insight into the classical response function may be obtained by deriving the identical result from a wholly classical mechanical treatment, which is based on the classical analogues of the approximations made in ref 28. We define a model classical oscillator by making a canonical transformation from the Morse action-angle variables of eqs 2.7−2.12 to a pair of "harmonic oscillator" variables

$$\bar{q}(I,\theta) = \sqrt{\frac{2I}{m\omega}}\cos\theta \quad (4.20a)$$

$$\bar{p}(I,\theta) = -\sqrt{2Im\omega}\sin\theta \quad (4.20b)$$

where the angle variable θ evolves under anharmonic Morse oscillator time evolution according to eq 2.11, $\theta(t) = \theta(0) + \bar{\omega}(I)t$, with I constant, and the action-dependent frequency defined in eq 2.12. This model oscillator is assumed to couple to the electromagnetic field through the "coordinate" $\bar{q}$, rather than q, so that the classical response function takes a form analogous but not identical to eq 2.3.

$$\bar{R}^{(3)}(t_3, t_2, t_1) = -\langle\{\{\{\bar{q}(t_3 + t_2 + t_1), \bar{q}(t_2 + t_1)\}, \bar{q}(t_1)\},$$
$$\bar{q}(0)\}\rangle \quad (4.21)$$

Equations 4.20 and 4.21 define a model anharmonic oscillator interacting with radiation, which is not identical to the Morse oscillator model of section II. The effective coordinate and

Vibrational Echoes

J. Phys. Chem. B, Vol. 108, No. 21, 2004 **6541**

momentum defined in eqs 4.20 may also be viewed as approximations to the Morse oscillator coordinate and momentum, obtained by expanding the exact relationships in eqs 2.8 and 2.9 to lowest order in H/D. The Fourier representation of the effective coordinate $\bar{q}(I,\theta) = \sum_k \bar{q}_k(I)e^{ik\theta}$ has only two terms, $k = \pm 1$, just as for a harmonic oscillator. This Fourier decomposition of $\bar{q}$ is, by standard correspondence principle arguments,[21] just the classical analogue of the restriction to one-quantum transitions ($\Delta n = \pm 1$) in the Akiyama–Loring treatment.[28] The nonlinearity of the oscillator is nevertheless manifested through the action dependence of $\bar{\omega}(I)$, the classical analogue of the anharmonic energy spacings preserved in the treatment of ref 28.

Using the expressions in eqs 4.20, it is possible to derive an explicit form for the nonlinear response $\bar{R}^{(3)}(t, 0, t)$. As the Fourier representation of the coordinate $\bar{q}(I,\theta;t)$ consists of two terms

$$\bar{q}(I, \theta; t) = \sqrt{\frac{I}{2m\omega}}[e^{+i\theta} e^{+i\bar{\omega}(I)t} + e^{-i\theta} e^{-i\bar{\omega}(I)t}] \quad (4.22)$$

evaluation of the nested Poisson brackets in eq 4.21 gives rise to a Fourier series with terms having $k = 0, \pm 2$, and ± 4. Those terms with $k \neq 0$ average to zero when integrated over the angle θ, so that only the $k = 0$ terms contribute to $\bar{R}^{(3)}$. For $t_1 = t$, $t_2 = 0$, and $t_3 = t$, the $k = 0$ terms are found to be

$$-\frac{t}{2m^2D}\Bigg[1 + 2\cos(2\bar{\omega}(I)t) + \frac{t^2I^2\omega^4}{2D^2}\cos(2\bar{\omega}(I)t) + \frac{3It\omega^2}{D}\sin(2\bar{\omega}(I)t)\Bigg] \quad (4.23)$$

The time-dependent phase factors in the nested Poisson bracket combine to give two types of terms, which, following the analysis of eqs 4.2 and 4.5, we designate as rephasing and nonrephasing, respectively. The rephasing term in eq 4.23 is $-t/2m^2D$ and has no oscillatory t dependence. The remaining terms are the nonrephasing contribution and exhibit oscillatory dependence in addition to power law growth in t. A diagrammatic representation of the classical response function in eq 4.21, which permits the ready identification of rephasing and nonrephasing contributions, is presented in the Appendix.

To compute $\bar{R}^{(3)}(t, 0, t)$, the $k = 0$ terms in eq 4.23 must be averaged over the action distribution function, $\rho(I)$. As the rephasing term is independent of action, its averaged value is $-t/2m^2D$ for an arbitrary normalized action distribution function. In particular, the rephasing term is independent of temperature. To evaluate the nonrephasing contributions to the response function, we employ the same approximations used in eqs 4.13–4.15 to obtain the $\hbar \to 0$ limit of the Akiyama–Loring theory; the Morse canonical distribution is replaced by the harmonic oscillator distribution $\rho_{HO}(I) = \omega\beta e^{-\omega\beta I}$, and the upper limit in the integration over action I is set to infinity. The classical nonlinear response function $\bar{R}^{(3)}(t, 0, t)$ is then found to be *identical* with the result obtained as the $\hbar \to 0$ limit of the Akiyama–Loring theory, namely, it is the sum of expressions 4.12 and 4.16, which is shown by the solid curve in Figure 4.

Although the nonrephasing terms in eq 4.23 diverge as powers of t for fixed values of the action I (energy $H(I)$), averaging over a distribution of frequencies $\bar{\omega}(I)$ leads to oscillatory contributions proportional to ratios of polynomials in t that decay to zero as $t \to \infty$. As noted in section III, the rephasing contribution linear in t has its origin in the behavior of two-

time Poisson brackets or stability matrix elements $\partial\bar{q}(t_a + t_b)/\partial\bar{p}(t_b)$; such linearity is generic for integrable systems[18] and can be understood in terms of the relative shearing motion of nearby trajectories in phase space. The manipulations that produced eq 4.23 give insight into the temperature independence of $R_{re}^{(3)}(t, 0, t)$ for the Morse oscillator. This is a consequence of the linear dependence of $\bar{\omega}(I)$ on I in eq 2.12. For the general case of a one-dimensional anharmonic oscillator, $\partial\bar{\omega}/\partial I$ is not constant, and the analogue of the first term in eq 4.23 will depend on action, thereby producing a temperature-dependent factor upon thermal averaging. As noted in the previous section, we have determined that the apparent linear divergence in $R_{cl}^{(3)}(t, 0, t)$ is temperature dependent for a quartic oscillator. The two analytic treatments of the nonlinear response of a Morse oscillator presented here support the existence of the apparent linear divergence manifested in the numerical calculations of Figures 2 and 4.

V. Conclusions

We have made three arguments in support of the proposition that the classical mechanical nonlinear response function for a thermal ensemble of anharmonic oscillators diverges in time. We have demonstrated this to be the case with numerical calculations over a finite time interval, and we have presented two derivations, from quantum and classical mechanics, of an approximate but quantitatively accurate theory that displays this feature. This finding brings together two notions that may be found in the literature. The first is the proposal by Leegwater and Mukamel[20] that the divergences that characterize classical mechanical nonlinear response functions for a microcanonical ensemble are destroyed by the dephasing associated with a thermal average in a canonical ensemble. The second is the textbook description[22,23] of echo spectroscopy as reversing the effects of inhomogeneous dephasing from a static distribution of energies. We propose that this rephasing property of the vibrational echo produces a divergence that is the signature of stabilities of classical trajectories.

What are the implications for molecules in the laboratory of this result for a model of noninteracting anharmonic oscillators? First, it must be recalled that the laboratory is quantum mechanical and that, at long enough time, apparent classical divergences turn into quantum oscillations, as in Figure 3. Second, our model has not included dissipation, which produces dephasing that is not rephased by the echo pulse sequence. However, the existence of a temporally diverging response function for the classical mechanical model considered here suggests that the time-dependent perturbation theory that produced eq 2.1 is not valid at long times for this model, because of the nonlinearity of classical mechanics. Such an interpretation is not without precedent. In his article entitled "The Case against Linear Response Theory," van Kampen has stated of nonlinear response theory that "this extension of linear response theory is even more manifestly wrong."[19] Fortunately, the practical utility of the results yielded by nonlinear response theory for dissipative systems with many degrees of freedom has been established empirically. Our finding has implications for finite-field calculations of the classical mechanical nonlinear response,[15–17] in which the complexities of relations containing stability matrices like eq 2.4 are avoided by carrying out nonequilibrium simulations in the presence of the driving field. For models of the type discussed here, the divergence of $R_{cl}^{(3)}$ suggests that the regime of validity of third-order response theory will become limited to weaker and weaker fields as time

6542 *J. Phys. Chem. B, Vol. 108, No. 21, 2004*

Noid et al.

increases. The practical implications of such a scenario remain to be explored in comparisons between finite-field and nonlinear response calculations in classical mechanics.

Appendix A: Diagrammatic Formulation of the Classical Response Function

In the calculation of the nonlinear response function for the classical model oscillator of eqs 4.20 and 4.21, the rephasing and nonrephasing contributions could be separately identified, as shown in eq 4.23. In the corresponding quantum mechanical calculation, double-sided Feynman diagrams[3,25] provide a useful way to identify rephasing and nonrephasing contributions to the response function. As noted previously, individual quantum mechanical double-sided Feynman diagrams diverge as $\hbar \to 0$ and hence have no direct classical mechanical analogues. However, the formalism of eqs 4.20 and 4.21 suggests a diagrammatic formulation of a classical response function, which retains the complex exponential functions characterizing coherence dynamics in quantum mechanics.

Because double-sided Feynman diagrams depict perturbations of the density matrix, we first rewrite the classical response function in eq 4.21 in an equivalent form in which Poisson brackets act directly on the classical phase space distribution, ρ.

$$\bar{R}^{(3)}(t_3, t_2, t_1) = -\int d\Gamma \, [\bar{q}(t_1 + t_2 + t_3)\{\bar{q}(t_1 + t_2), \{\bar{q}(t_1), \\ \{\bar{q}(0), \rho\}\}\}] \quad (A1)$$

For a single degree of freedom, the phase space volume element $d\Gamma = dp \, dq$ can be written through a canonical transformation in the action-angle variables of eqs 2.8−2.12 as $d\Gamma = dI \, d\theta$. The effective coordinate in eq 4.22 may be written as

$$\bar{q}(I, \theta; t) = q_\uparrow + q_\downarrow \quad (A2)$$

$$q_\uparrow = \sqrt{\frac{I}{2m\omega}} \, e^{i\theta} \, e^{i\omega t} \, e^{-i\omega^2 I t/2D}, \quad q_\downarrow = q_\uparrow^* \quad (A3)$$

Substitution of this Fourier series for $\bar{q}$ into the four occurrences of that quantity in eq A1 yields 16 terms. Each occurrence of $q_\uparrow$ carries a factor $\exp(i\theta)$, and each $q_\downarrow$ contributes $\exp(-i\theta)$. Terms in the integrand in eq A1 that carry a factor $\exp(ik\theta)$ with $k \neq 0$ will average to zero, because the distribution is independent of θ. Therefore, out of the 16 terms, only the 6 terms involving two factors each of $q_\uparrow$ and $q_\downarrow$ will survive the angle average. These terms can be represented with the six diagrams shown in Figure 5. Each diagram is read from left to right, with successive line segments representing the effects of $\bar{q}(0)$, $\bar{q}(t_1)$, $\bar{q}(t_1 + t_2)$, and $\bar{q}(t_1 + t_2 + t_3)$. Thus, the three leftmost segments represent Poisson brackets, and the rightmost segment indicates multiplication. Segments pointing up, as scanned from left to right, indicate $q_\uparrow$, and segments pointing down represent $q_\downarrow$. For example, diagram I in Figure 5 represents the term

$$I = -\int d\Gamma \, [q_\uparrow(t_1 + t_2 + t_3)\{q_\downarrow(t_1 + t_2), \{q_\downarrow(t_1), \{q_\uparrow(0), \rho\}\}\}] \quad (A4)$$

Each graph must begin and end on a (hypothetical) horizontal
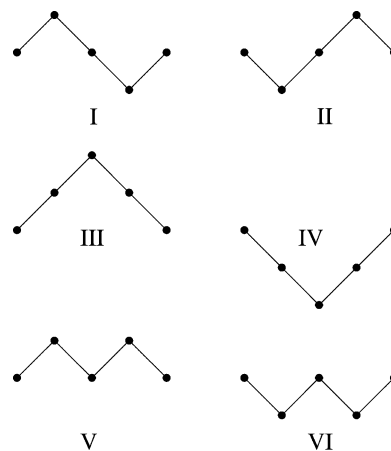

Figure 5. Diagrammatic representation of a classical mechanical nonlinear response function.

line connecting the endpoints. Graphs related by reflection about this horizontal line have values that are complex conjugates, for example, $I = II^*$. Each graph, at $t_2 = 0$, represents either a rephasing or nonrephasing contribution to the vibrational echo.

From eq A3, each $q_\uparrow(t)$ carries a phase factor $\exp(i\omega t)$, while $q_\downarrow(t)$ carries $\exp(-i\omega t)$. The total phase factor associated with each diagram is then easily determined. Diagram I in Figure 5 has the phase factor $\exp(i\omega(t_3 - t_1))$ and is by definition a rephasing contribution. Diagram II has a value that is the complex conjugate of that of I and has phase factor $\exp(-i\omega(t_3 - t_1))$. Diagrams III−VI represent nonrephasing contributions, with phase factors $\exp(\pm i\omega(t_3 + t_1))$. The value of diagram I is

$$I(t_3, 0, t_1) = \left(\frac{-t_3}{4m^2D}\right) e^{i\omega(t_3 - t_1)} \left[\bar{N}_0^*(t_3 - t_1) - \\ i\frac{\omega(2t_3 - t_1)}{2\beta D}\bar{N}_1^*(t_3 - t_1) - \frac{\omega^2 t_3(t_3 - t_1)}{8\beta^2 D^2}\bar{N}_2^*(t_3 - t_1)\right] \quad (A5)$$

The dephasing functions $\bar{N}_j$ are defined in eq 4.9. The values of the other five diagrams can be related to that of I according to

$$II(t_3, 0, t_1) = I^*(t_3, 0, t_1)$$

$$III(t_3, 0, t_1) = I^*(t_3, 0, -t_1)$$

$$IV(t_3, 0, t_1) = I(t_3, 0, -t_1) \quad (A6)$$

$$V(t_3, 0, t_1) = I^*(t_3, 0, -t_1)$$

$$VI(t_3, 0, t_1) = I(t_3, 0, -t_1)$$

Summing the graphs yields

$$R_{re}(t_3, 0, t_1) = 2\text{Re} \, I(t_3, 0, t_1)$$

$$R_{nr}(t_3, 0, t_1) = 2R_{re}(t_3, 0, -t_1) \quad (A7)$$

Substitution of the value of I in eq A5 into eqs A7 gives the expressions in eqs 4.10 and 4.11. Although the specific results in eqs A5−A7 were derived for the particular case of the Morse oscillator, this diagrammatic representation of the third-order response function is applicable to general potentials, within the approximation of the coordinate by the quantity $\bar{q}$ in eq 4.20. The diagrammatic formulation in Figure 5 permits the applica-

tion of the quantum mechanical concepts "rephasing" and "nonrephasing" in classical mechanics.

References and Notes

(1) Mukamel, S.; Piryatinski, A.; Chernyak, V. *Acc. Chem. Res.* **1999**, *32*, 145−154.

(2) Fayer, M. D. *Annu. Rev. Phys. Chem.* **2001**, *52*, 315−356.

(3) Hamm, P.; Lim, M.; Hochstrasser, R. M. *Phys. Rev. Lett.* **1998**, *81*, 5326−5329.

(4) Wright, J. C. *Int. Rev. Phys. Chem.* **2002**, *21*, 185−255.

(5) Golonzka, O.; Khalil, M.; Demirdoven, N.; Tokmakoff, A. *J. Chem. Phys.* **2001**, *115*, 10814−10828.

(6) Kaufman, L. J.; Heo, J. Y.; Ziegler, L. D.; Fleming, G. R. *Phys. Rev. Lett.* **2002**, *88*, 207402.

(7) Piryatinski, A.; Skinner, J. L. *J. Phys. Chem. B.* **2002**, *106*, 8055−8063.

(8) Mukamel, S.; Khidekel, V.; Chernyak, V. *Phys. Rev. E* **1996**, *53*, R1−R4.

(9) Keyes, T.; Fourkas, J. T. *J. Chem. Phys.* **2000**, *112*, 287−293.

(10) Williams, R. B.; Loring, R. F. *J. Chem. Phys.* **2000**, *113*, 1932−1941.

(11) Williams, R. B.; Loring, R. F. *J. Chem. Phys.* **2000**, *112*, 3104−3105.

(12) Williams, R. B.; Loring, R. F. *Chem. Phys.* **2001**, *266*, 167−176.

(13) Wu, J.; Cao, J. *J. Chem. Phys.* **2001**, *115*, 5381−5391.

(14) Ma, A.; Stratt, R. M. *J. Chem. Phys.* **2002**, *116*, 4602−4971.

(15) Dellago, C.; Mukamel, S. *Phys. Rev. E* **2003**, *67*, 035205.

(16) Saito, S.; Ohmine, I. *Phys. Rev. Lett.* **2002**, *88*, 207401.

(17) Saito, S.; Ohmine, I. *J. Chem. Phys.* **2003**, *119*, 9073−9087.

(18) Lichtenberg, A. J.; Lieberman, M. A. *Regular and Chaotic Dynamics*, 2nd ed.; Springer-Verlag: New York, 1992.

(19) van Kampen, N. G. *Phys. Norv.* **1971**, *5*, 279−284.

(20) Leegwater, J. A.; Mukamel, S. *J. Chem. Phys.* **1995**, *102*, 2365−2371.

(21) Child, M. S. *Semiclassical Mechanics with Molecular Applications*; Oxford University Press: New York, 1991.

(22) Steinfeld, J. I. *Molecules and Radiation: an Introduction to Modern Molecular Spectroscopy*; MIT Press: Cambridge, MA, 1985.

(23) Fleming, G. R. *Proc. Natl. Acad. Sci. U.S.A.* **1998**, *95*, 15161−15162.

(24) Noid, W. G.; Ezra, G. S.; Loring, R. F. *J. Chem. Phys.* **2003**, *119*, 1003−1020.

(25) Mukamel, S. *Principles of Nonlinear Optical Spectroscopy*; Oxford University Press: New York, 1995.

(26) Sage, M. *Chem. Phys.* **1978**, *35*, 375−380.

(27) Shirts, R. B. *J. Phys. Chem.* **1987**, *91*, 2258−2267.

(28) Akiyama, R.; Loring, R. F. *J. Chem. Phys.* **2002**, *116*, 4655−4664.